RSC Advances

ROYAL SOCIETY OF CHEMISTRY

www.rsc.org/advances

Coordination assemblies of the M^{II}-tm/bpt (M = Zn/Cd/Co/Ni) mixed-ligand system: positional isomeric effect, structural diversification and properties

Fu-Ping Huang,[ab] Peng-Fei Yao,[a] Wei Luo,[a] Hai-Ye Li,[a] Qing Yu,[a] He-Dong Bian,[a] Shi-Ping Yan,*[b]*

ABSTRACT:

To further investigate the influence of the positional isomeric ligands on the structural topologies, six new coordination polymers with three positional isomeric dipyridyl ligands (4,4'-Hbpt, 3,4'-Hbpt and 3,3'-Hbpt) and trimellitic acid (H_3tm), namely, $\{[Zn_3(tm)_2(4,4'\text{-Hbpt})_2(H_2O)_2]\cdot 10H_2O\}_n$ **(1)**, $[Zn_3(tm)_2(3,3'\text{-Hbpt})_2]_n$ **(2)**, $\{[Cd_2(tm)(3,4'\text{-bpt})(H_2O)_2]\cdot H_2O\}_n$ **(3)**, $\{[Cd_4(tm)_2(3,3'\text{-bpt})_2(H_2O)_2]\cdot 3H_2O\}_n$ **(4)**, $\{[Co_3(tm)_2(3,4'\text{-Hbpt})_2(H_2O)_6]\cdot 2H_2O\}_n$ **(5)**, $\{[Ni_3(tm)_2(3,3'\text{-Hbpt})_4(H_2O)_2]\cdot 7H_2O\}_n$ **(6),** have been synthesized under hydrothermal conditions and characterized**.** Structural analysis reveals that: **1** and **5** both have 3D 4-connected networks, with $(4.6^4.8)(4^2.6^3.8)_2(4^4.6^2)_2$ Schläfli symbol for **1** and $(4^2.5^2.7^2)(5^2.6^2.7.8)_2(4.5^2.6.7^2)_2$ symbol for **5**, respectively. **2** and **3** both have 3D (4, 5)-connected networks, with $(3^4.4^2.5^2)_2(4^2.8^4)(3.4^3.5^2.6.7^2.8)_2$ symbol for **2** and $(3^4.4^2.5^2)_2(4^2.8^4)(3.4^3.5^2.6.7^2.8)_2$ symbol for **3**, respectively. **4** has a 3D trinodal (3,4,5)-connected net with $(3.4^4.5^3.6.7)(4^3.6^2.7)(4^4.6^2)(4^2.6)_2(4^5.6^4.8)_2$ symbol. **6** has a 2D (3, 4)-connected layer with $(3.6^2)_2(3.4.6^2.7^2)_2(5.6^3.8^2)$ symbol. These results indicate that the versatile coordination modes of tm and the isomeric nature of bpt play crucial roles in modulating structural topologies of these complexes. Moreover, the luminescent properties of **1**−**4** and the magnetic behavior of **5**−**6**, have been investigated.

[a] *Key Laboratory for the Chemistry and Molecular Engineering of Medicinal Resources (School of Chemistry and Pharmacy, Guangxi Normal University), Ministry of Education of China, Guilin, 541004, P. R. China. Email: gxunchem@163.com;*

[b] *Department of Chemistry, Nankai University, Tianjin 300071, PR China* Email: *yansp@nankai.edu.cn;*

Introduction

The design and construction of coordination polymers have achieved considerable interest in the realm of crystal engineering, not only for their tremendous potential applications as functional materials,[1-6] but also for their intriguing variety of topological structures.[7-10] The structural natures are diverse depending on the metal ions, PH value, solvents, the ligands, synthetic methods, etc.[11-13] One of the most useful and important way to study the controllable construction is still the deliberate modifications on the organic ligands.[14-15] Among the reported studies, much effort has been focused on the construction of coordination polymers using multidentate ligands such as polycarboxylate and N-heterocyclic ligands.[16] Recently, Our group had reported a series of $Co^{II}/Zn^{II}/Cd^{II}$ coordination polymers with different topological structures based on the mixed-ligand systems of three positional isomeric N-heterocyclic-like ligands: 1H-3,5-bis(4-pyridyl)-1,2,4-triazole (4,4′-Hbpt), 1H-3-(3-pyridyl)-5-(4-pyridyl)-1,2,4-triazole (3,4′-Hbpt), 1H-3,5-bis(3-pyridyl)-1,2,4 -triazole (3,3′-Hbpt) and three positional isomeric aromatic dicarboxylic anions: the *o*-BDC, *m*-BDC, *p*-BDC (BDC = benzenedicarboxylate anion).[17]

As an extension of this work, we choose trimellitic acid (H_3tm) and the above-mentioned isomeric N-heterocyclic ligands, to construct new coordination frameworks with versatile topological symbol. Tm with versatile coordination modes, can be considered as a bent building block like *o*, *m*-BDC, and a linear building block like *p*-BDC (Scheme 1). A series of coordination polymers, namely, $\{[Zn_3(tm)_2(4,4'\text{-Hbpt})_2(H_2O)_2]\cdot 10H_2O\}_n$ **(1)**, $[Zn_3(tm)_2(3,3'\text{-Hbpt})_2]_n$ **(2)**, $\{[Cd_2(tm)(3,4'\text{-bpt})(H_2O)_2]\cdot H_2O\}_n$ **(3)**, $\{[Cd_4(tm)_2(3,3'\text{-bpt})_2(H_2O)_2]\cdot 3H_2O\}_n$ **(4)**, $\{[Co_3(tm)_2(3,4'\text{-Hbpt})_2(H_2O)_6]\cdot 2H_2O\}_n$ **(5)**, $\{[Ni_3(tm)_2(3,3'\text{-Hbpt})_4(H_2O)_2]\cdot 7H_2O\}_n$ **(6)** were constructed successfully. The positional isomeric effects of the bpt bridges on the coordination assemblies were elucidated. In addition, the magnetic and luminescent properties of these compounds have been investigated.

Scheme 1

Experimental Section

Materials and Physical Measurements

With the exception of the ligands of 4,4′-Hbpt, 3,4′-Hbpt, and 3,3′-Hbpt, which were prepared according to the literature procedure,[18] all reagents and solvents for synthesis and analysis were commercially available and used as received. IR spectra were taken on a Perkin-Elmer spectrum One FT-IR spectrometer in the 4000-400 cm^{-1} region with KBr pellets. Elemental analyses for C, H and N were carried out on a Model 2400 II, Perkin-Elmer elemental analyzer. The magnetic susceptibility measurements of the polycrystalline samples were measured over the temperature range of 2-300K with a Quantum Design MPMS-XL7 SQUID magnetometer using an applied magnetic field of 1000 Oe. Field dependences of magnetization were measured using a flux magnetometer in an applied field up to 50 kOe generated by a conventional pulsed technique. A diamagnetic correction to the observed susceptibilities was applied using Pascal's constants. X-ray powder diffraction (XRPD) intensities were measured on a Rigaku D/max-IIIA diffractometer (*Cu-Kα*, λ = 1.54056 Å). The single crystalline powder samples were prepared by crushing the crystals and scanned from 3 to 60^{o} with a step of 0.1^{o}/s. Calculated patterns of **1-6** were generated with PowderCell.

Syntheses of complexes 1–6

$\{[Zn_3(tm)_2(4,4'\text{-}Hbpt)_2(H_2O)_2]\cdot 10H_2O\}_n$ (1). A mixture containing H_3tm (105 mg，0.5mmol)，$Zn(NO_3)_2\cdot 6H_2O$ (149 mg，1 mmol), 4,4′-Hbpt (112 mg, 0.5 mmol), NaOH (40 mg, 1 mmol), water(10 mL) and ethanol (5 mL) was sealed in a Teflon-lined stainless steel vessel (23 mL), which was heated at 140 ^{o}C for 3 days and then cooled to room temperature at a rate of 5 ^{o}C/h. Colorless block crystals of **1** were obtained and picked out, washed with distilled water and dried in air. Yield: 48% (based on Zn(II)). Elemental analysis for $C_{42}H_{50}N_{10}Zn_3O_{24}$ (%) Calcd: C, 39.56; H, 3.95; N, 10.98. Found: C, 39.97; H, 3.27; N, 10.52. IR (KBr, cm^{-1}): 3421s, 1623s, 1556s, 1411s, 1314s, 1055m, 841w, 608m.

$[Zn_3(tm)_2(3,3'\text{-}Hbpt)_2]_n$ (2). A mixture containing H_3tm (105 mg，0.5mmol)，$Zn(NO_3)_2\cdot 6H_2O$ (149 mg，1 mmol), 3,3′-Hbpt (112 mg, 0.5 mmol), NaOH (40 mg, 1 mmol) and water (10 mL) was sealed in a Teflon-lined stainless steel vessel (23 mL), which was heated at 140 ^{o}C for 3 days and then cooled to room temperature at a rate of 5 ^{o}C/h. Colorless block crystals of **2** were obtained and picked out, washed with

distilled water and dried in air. Yield: 34% (based on Zn(II)). Anal. Calcd for ($C_{42}H_{24}N_{10}Zn_3O_{12}$): C, 47.73; H, 2.29; N, 13.25. Found: C, 47.79; H, 3.00; N, 13.52. IR (KBr, cm^{-1}): 3401s, 1611s, 1543s, 1403s, 1343s, 1067m, 845w, 611m.

{[Cd_2(tm)(3,4′-bpt)(H_2O)$_2$]·H_2O}$_n$ (3), The same synthetic procedure as that for **2** was used except that $Zn(NO_3)_2·6H_2O$ and 3,3′-Hbpt was replaced by $Cd(Ac)_2·2H_2O$ and 3,4′-bpt, respectively, giving colorless block X-ray-quality crystals of **3** in a 40% yield (based on Cd (II)). Anal. Calcd for ($C_{21}H_{17}Cd_2N_5O_9$): C, 35.61; H, 2.42; N, 9.89. Found: C, 35.81; H, 2.50; N, 9.97. IR (KBr, cm^{-1}): 3396m, 1615m, 1585s, 1492w, 1384s, 1067m, 823w, 790w, 738w.

{[Cd_4(tm)$_2$(3,3′-bpt)$_2$(H_2O)$_2$]·3H_2O}$_n$ (4), The same synthetic procedure as that for **2** was used except that $Zn(NO_3)_2·6H_2O$ was replaced by $Cd(Ac)_2·2H_2O$ giving colorless block X-ray-quality crystals of **4** in a 38% yield (based on Cd (II)). Anal. Calcd for ($C_{42}H_{28}Cd_4N_{10}O_{15}$): C, 37.03; H, 2.07; N, 10.28. Found: C, 37.19; H, 2.10; N, 10.52. IR (KBr, cm^{-1}): 3401m, 1583w, 1561s, 1536w, 1372s, 1166m, 853m, 831m, 768m, 752w, 702m, 571m.

{[Co_3(tm)$_2$(3,4′-Hbpt)$_2$(H_2O)$_6$]·2H_2O}$_n$ (5). The same synthetic procedure as that for **1** was used except that $Zn(NO_3)_2·6H_2O$ and 4,4′-Hbpt was replaced by $Co(NO_3)_2·6H_2O$ and 3,4′-bpt, respectively, giving red columnar X-ray-quality crystals of **5** in a 34% yield (based on Co(II)). Anal. Calcd for ($C_{42}H_{40}Co_3N_{10}O_{20}$): C, 42.69; H, 3.41; N, 11.85. Found: C, 42.57; H, 3.72; N, 11.52. IR (KBr, cm^{-1}): 3402s, 1613s, 1576s, 1412s, 1348s, 1055m, 845w, 613m.

{[Ni_3(tm)$_2$(3,3′-Hbpt)$_4$(H_2O)$_2$]·7H_2O}$_n$ (6). The same synthetic procedure as that for **2** was used except that $Zn(NO_3)_2·6H_2O$ was replaced by $Ni(NO_3)_2·6H_2O$ giving green block X-ray-quality crystals of **6** in a 44% yield (based on Ni(II)). Anal. Calcd for ($C_{66}H_{62}N_{20}Ni_3O_{22}$): C, 47.65; H, 3.76; N, 16.84. Found: C, 47.57; H, 3.72; N, 16.52. IR (KBr, cm^{-1}): 3412s, 1632s, 1556s, 1421s, 1344s, 1051m, 842w, 608m.

X-ray Crystallographic Determination

All reflection data were collected on a Bruker SMART CCD instrument by using graphite-monochromatic *Mo-Kα* radiation (λ = 0.71073 Å) at room temperature. A semiempirical absorption correction by using the SADABS program was applied, and the raw data frame integration was performed with SAINT[19]. The crystal structures were solved by the direct method using the program SHELXS-97[20] and refined by the full-matrix least-squares method on F^2 for all non-hydrogen atoms using

SHELXL-97[21] with anisotropic thermal parameters. All hydrogen atoms were located in calculated positions and refined isotropically, except the hydrogen atoms of water molecules were fixed in a difference Fourier map and refined isotropically. The details of the crystal data were summarized in Table 1, and selected bond lengths and angles for compounds **1−6** are listed in Table 2. The crystallographic data of **1–6** in CIF format has been deposited in the Cambridge Crystallographic Data Center (CCDC reference number: 916306 - 916311).

Table 1

Table 2

XRPD Results

To confirm whether the crystal structures are truly representative of the bulk materials, X-ray powder diffraction (XRPD) experiments have also been carried out for **1-6**. The XRPD experimental and computer-simulated patterns of the corresponding complexes are shown in ESI, Figure S2-S7, Supporting Information. Although the experimental patterns have a few unindexed diffraction lines and some are slightly broadened in comparison with those simulated from the single crystal models, it can still be considered favorably that the bulk synthesized materials and the as-grown crystals are homogeneous for **1-6**.

Results and Discussion

Crystal structures

$\{[Zn_3(tm)_2(4,4'\text{-Hbpt})_2(H_2O)_2]\cdot 10H_2O\}_n$ (1). As shown in Fig. 1a, **1** reveals a novel 3D coordination polymer with a V-shaped trinuclear Zn(II) unit bridged by tm anions. In the trinuclear unit, the middle Zn1 ions lying on a twofold axis exhibit a four-coordinated tetrahedrally environment with two carboxylic O atoms (O1, O1A, Symmetry code: A: -*x*, *y*, -*z*+1/2) from two tm anions and two N atoms (N1, N1A) from two 4,4′-Hbpt ligands. The terminal Zn2 ions exhibit a distorted octahedral geometry, which is provided by one pyridyl N (N5B, B: *x*-1, -*y*+1, *z*+1/2) donor, four carboxylate O (O2, O3A, O5C, O6C, C: -*x*+1/2, -*y*+1/2, -*z*+1) atoms and one water molecule (O7). The middle Zn1 ion is linked to terminal Zn2 ions with one *syn–anti*

carboxylate from tm [Zn···Zn = 4.411(1) Å] to form the V-shaped unit. The adjacent trinuclear units are linked by tm to generate straight-like chains running along the crystallographic *c* axis (Fig. 1b), in which tm exhibit a coordinating mode of mode 1 (Scheme 1) and three carboxylate groups of tm exhibit three different coordination patterns (unidentate, chelating, and *syn-anti* bridge modes, respectively). On the other hand, the adjacent trinuclear units are bridged by 4,4′-bpt ligands to result in zigzag-like chains along the *a* axis (Fig. 1c).

As a consequence, the adjacent trinuclear units are further connected by tm and 4,4′-Hbpt components, resulting into the generation of a 3D coordination polymeric network (Fig. 1d). A topological analysis reveals that each tm serves as a 4-connected node to join four Zn(II) ions, both Zn1 and Zn2 play the 4-connected role to link each other *via* the 4,4′-Hbpt spacers and tm nodes. According to Wells' topology definition[22], an unprecedented 4-connected topology with the short Schläfli symbol of $(4.6^4.8)(4^2.6^3.8)_2(4^4.6^2)_2$ is formed (Fig. 1e). Considering the trinuclear Zn(II) unit as a node to simply the structure of **1**, simplified topologie could also be determined with the short Schläfli symbol of $5^2.6^4$ (Fig. 1f). Interestingly, the void space in the single framework is so large that there identical 3D frameworks interpenetrate each other, leaving a small space for the inclusion of solvent water molecules.

Fig. 1

$[Zn_3(tm)_2(3,3'\text{-Hbpt})_2]_n$ (2). The asymmetric unit of **2** consists of two Zn(II) ions, the Zn1 ion adopts a slightly distorted trigonal-dipyramidal geometry surround by two N atoms (N1, N5B, B: -*x*+3/2, -*y*+3/2, -*z*+1) from two 3,3′-Hbpt ligands in the axial position, three O atoms (O1, O5A, O6B, A: *x*+1/2, *y*-1/2, *z*) from three tm anions in the equatorial plane. The Zn2 center lying on a twofold axis has a tetrahedron geometry from four carboxylate O atoms (O2C, O2D, O3, O3E, C: *x*-1/2, *y*+1/2, *z*; D: -*x*+3/2, *y*+1/2, -*z*+3/2; E: -*x*+1, *y*, -*z*+3/2) (Fig. 2a). Tm in **2** exhibit a coordinating mode of mode 2 (Scheme 1), and three carboxylate groups of tm exhibit three different coordination patterns: one is in monodentate fashion, another group bridge two Zn(II) centers in *syn-syn* mode to form a binuclear Zn(II) unit (Zn···Zn = 3.767 (2) Å), leading to a 1-D chain along the crystallographic *c* axis (Fig. 2b), and the third carboxylate group adopts a *syn–anti* mode bridging adjacent Zn(II) atoms with the Zn···Zn separation of 4.172 (2) Å. The adjacent Zn(II) centers in **2** are connected by tm

components, resulting into the generation of a 3D [Zn(tm)] coordination polymeric network (Fig. 2c). In addition, the 3D [Zn(tm)] network are further fixed by 3,3′-Hbpt ligands with *syn-syn* mode bridging the adjacent Zn(II) atoms. (Fig. 2d).

Fig. 2

On the basis of the connectivity of Zn1 and Zn2 atoms, both of them are viewed to be 4-connected nodes. Moreover, tm also can be viewed as a 4-connected node and the 3,3′-Hbpt as a linker. In this way, this framework can be simplified to be a 4-connected topology with the short Schläfli symbol of $(3^4.4^2.5^2)_2(4^2.8^4)(3.4^3.5^2.6.7^2.8)_2$ (Fig. 2e). Considering the dinuclear Zn(II) unit bridged by tm anions as a node to simply the structure of **2**, simplified topologies could also be determined with the short Schläfli symbol of $(4^4.6^2)$ $(4^8.6^6.8)$ (Fig. 2f).

$\{[Cd_2(tm)(3,4'\text{-bpt})(H_2O)_2]\cdot H_2O\}_n$ (3). **3** features a 3D coordiation polymeric architecture, containing two independent Cd(II) cations (Fig. 3a). The Cd1 ion is coordinated by one pyridyl N donor (N1C, C: -*x*+1, -*y*+1, -*z*+2), one triazole N donor (N3), and four carboxylate O atoms (O1B, O2B, O4A, O5, A: *x*+1, -*y*, -*z*+1; B: -*x*+1, -*y*+1, -*z*+1), to form a distorted octahedral geometry. The Cd2 ion also adopts a distorted octahedral geometry, which is provided by one triazole N atom of 3,4′-bpt (N4) and one water O atom (O8), two carboxylate O atoms (O3A, O5) from two tm anions, one water O atom (O7) and one pyridyl N atom 3,4′-bpt (N5D, D: -*x*+2, -*y*, -*z*+2). The Cd2 ion is linked to Cd1 ion with mixed bridges through one μ_2 carboxyl O atom, one *syn-syn* carboxylate [Cd···Cd = 3.5739(9)Å, Cd1—O5—Cd2 = 101.84(2)°] and two triazole N atoms to form a dinuclear unit. The adjacent dinuclear units are linked by tm to generate a 1-D chain running along the crystallographic *b* axis (Fig. 3b). Tm in **3** exhibit a coordinating mode of mode 3 (Scheme 1). And three carboxylate groups on the tm anion of the 1-D chain display different coordination patterns (μ_2-carboxyl O, chelating, and *syn-syn* bridge modes, respectively). The 3,4′-bpt ligand exhibit a coordinating mode of μ_4-η^1:η^1:η^1:η^1. The adjacent dinuclear units are also connected by 3,4′-bpt ligand to generate a 1D chain (Fig. 3c). As a consequence, adjacent dinuclear units are connected by tm and 3,4′-bpt ligand, resulting into the generation of a 3D coordination polymeric network (Fig. 3d).

A better insight into the nature of this 3D coordination polymeric network can be achieved by topological analysis, as shown in Fig. 3e. In **3**, Cd1 and Cd2 atoms can be

viewed as 5-connected and 4-connected nodes, respectively. And the 3D network can be further simplified by considering tm as 5-connected nodes and 3,4′-bpt as 4-connected nodes, respectively. Thus, the structure can be simplified as a (4, 5)-connected topology with $(3.4^4.5.6^3.8)(3.4^3.6^2)(3^3.4^4.5.6^2)(4^3.6^2.8)$ Schläfli symbol. Considering the dinuclear Cd(II) unit as a node to simply the structure of **3**, simplified topologies could also be determined with the short Schläfli symbol of $(4^2.6)$ $(4^2.6^5.8^3)$ (Fig. 3f). Different from bpt ligands reported before,[17] which act as linkers, the 3,4′-bpt ligands in **3** act as a 4-connected node, with two triazolyl nitrogen donors coordinating with two Cd atoms. As a result, compound **3** reveals a more complicated architecture than before.

Fig. 3

$\{[Cd_4(tm)_2(3,3'\text{-bpt})_2(H_2O)_2]\cdot 3H_2O\}_n$ (4). The asymmetric unit of **4** consists of four Cd(II) cations. As shown in Fig. 4a, Cd1 and Cd2 are displaying slightly distorted octahedral geometry, while Cd3 and Cd4 showing distorted tetragonal-pyramidal environment. The Cd1 ion is defined by five carboxylate O atoms (O1, O2, O3B, O4A, O9C, A: $x-1$, y, z; B: $-x+2$, $-y+1$, $-z+1$; C: $x+1$, y, z) and one pyridyl N atoms (N1) of 3,3′-bpt; the coordination sites of Cd2 are occupied by four carboxylate O atom (O4A, O7, O8, O9C), one water O atoms (O13) and one pyridyl N atoms (N6) of 3,3′-bpt ligand; the Cd3 ion is coordinated by two carboxylate O atoms (O7, O11C) of two tm ligands, one water oxygen atoms (O14) and two N atoms (N4, N5D, D: $-x$, $-y$, $-z$) from two 3,3′-bpt ligands; the coordination sphere of Cd4 is made up of two carboxylate O atom (O5A, O6A) from one tm ligand, one water O atoms (O15) and two pyridyl N donor (N8, N10E, E: $-x+2$, $-y+2$, $-z+1$) from two 3,3′-bpt ligands. In addition, the distance of Cd4 and O2 is 2.777(8)Å indicating a weak interaction. Tm in **4** exhibits two kinds of different coordinating modes: mode 4 and mode 5 (Scheme 1). The different modes of the tm is conducive to the formation of the centrosymmetric structural framework of **4**. It is quite interesting that, tm adopt aforementioned coordinating modes, link the Cd(II) atoms to form a decorated ribbon chains along the *a* axis (Fig. 4b). In the middle of the chain, tm adopt mode 4. While on both sides of the chain tm adopt mode 5. The chain possesses a certain width because tm keeps two uncoordinated oxygen atoms outside the chain in mode 5, characteristics which are relatively rare in the reported articles.[23] Then, the chain are cross-linked by pyridine N

atoms and triazole N atoms of 3,3′-bpt ligands to generate a 3D network (Fig. 4c).

Fig. 4

Considering of the connectivity of Cd atoms, Cd1 can be viewed as a 5-connected node, Cd2 and Cd3 are viewed as 4-connected nodes and Cd4 atom as 3-connected node, respectively (the ratio is 1:2:1). Thus, this 3D network can be further simplified by considering each tm as a 5-connected node and each 3,3′-bpt ligand as a 3-connected node. Therefore, the overall structure of **4**, can be simplified as a trinodal (3,4,5)-connected net with the short Schläfli symbol of $(3.4^4.5^3.6.7)(4^3.6^2.7)(4^4.6^2)(4^2.6)_2(4^5.6^4.8)_2$ (Fig. 4d). Considering the dinuclear Cd(II) unit as a node to simply the structure of **3**, simplified topologies could also be determined with the short Schläfli symbol of $(3^2.4^2.5^2)(3^2.4^5.5^6.6^2)_2$ (Fig. 4e). Different from compound **3**, the 3,3′-bpt ligands in **4** act as a 3-connected node, with a triazolyl nitrogen donor coordinating with a Cd atom. As a result, compound **4** also reveals a more complicated architecture than before[17].

$\{[Co_3(tm)_2(3,4'\text{-}Hbpt)_2(H_2O)_6]\cdot 2H_2O\}_n$ (5). The asymmetric unit of **5** contains three independent Co(II) cations with octahedron coordination spheres (Fig. 5a). And all of the Co atoms lie on independent inversion centres. The Co1 center is coordinated by four equatorial carboxylate/water O atoms (O1, O1A, O7, O7A, A: -*x*+2, -*y*, -*z*+1) and two apical carboxylate O atoms (O6B, O6C, B: *x*-1, *y*, *z*; C: -*x*+3, -*y*, -*z*+1). Co2 is coordinated by two water moleculars (O8, O8A) and two pyridyl N atoms (N5E, N5F, E: -*x*+1, -*y*, -*z*; F: *x*+1, *y*-1, *z*+1) in the equatorial plane, two carboxylate O atoms (O2, O2D, D: -*x*+2, -*y*-1, -*z*+1) in the axial position. Co3 is coordinated by two carboxylate O atoms (O3, O3G, G: -*x*+2, -*y*, -*z*) and two pyridyl N atoms (N1, N1G) in the equatorial plane, two water moleculars (O9, O9G) in the axial position.

Fig. 5

Tm in **5** exhibits a coordinating mode of mode 6 (Scheme 1). Three carboxylic groups of tm exhibit two kinds of coordination modes: one carboxylate group adopts a *syn–anti* bridging mode to connect the adjacent Co(II) cations with a separation of 5.011 (2) Å to furnish a 1-D chain along the *b* axis whereas the other two carboxylate groups are monodentate. As a consequence, the adjacent Co(II) centers are connected

by tm components, resulting in the generation of a 3D coordination polymeric network (Fig. 5b). In addition, the 3D Co-tm network are further fixed by 3,4′-Hbpt ligands through bridging the adjacent Co atoms (Fig. 5c). From a topology view, all of the Co1, Co2, Co3 and tm can be viewed as 4-connected nodes, and the 3,4′-Hbpt can be viewed as a linker. As a result, this framework can be simplified as a 4-connected topology with the short Schläfli symbol of $(4^2.5^2.7^2)(5^2.6^2.7.8)_2(4.5^2.6.7^2)_2$ (Fig. 5d).

$\{[Ni_3(tm)_2(3,3'\text{-}Hbpt)_4(H_2O)_2]\cdot 7H_2O\}_n$ (6). **6** reveals a novel 2D coordination polymer with a linear trinuclear Ni(II) unit. The asymmetric unit of **6** has one and a half crystallographically independent Ni atoms (Ni2 lies on a symmetry site). Both of them display slightly distorted octahedral coordination geometries (Fig. 6a). The Ni1 center is coordinated by three carboxylate O atoms from three tm anions (O1, O7, O4A, A: -*x*+1, -*y*, -*z*+2, Ni1—O = 2.026(6)-2.096(6) Å) and three N atoms from three 3,3′-Hbpt ligands (N1, N5A, N6, Ni1—N = 2.108(8)-2.133(8) Å). Ni2 lying on an inversion centre is coordinated by four carboxylate O atoms from two tm anions (O3, O3B, O5, O5B, B: -*x*+1, -*y*-1, -*z*+2, Ni2—O = 2.072(6)-2.082(7) Å) and two pyridyl N donors from two 3,3′-Hbpt ligands (N10C, N10D, C: *x*-1, *y*-1, *z*+1, D: -*x*+2, -*y*, -*z*+1, Ni2—N = 2.086(8) Å). The middle Ni2 ion is linked to two terminal Ni1 atoms with one *syn*−*anti* carboxylate from tm with a separation of 5.373(1) Å to furnish a linear trinuclear Ni(II) unit (Fig.6d). These Ni_3 subunits are further extended by tm into a 1D chain along the b axis (Fig. 6b) in which tm exhibit a coordinating mode of mode 7 (Scheme 1) and three carboxylate groups of tm exhibit two different coordination patterns (unidentate and *syn-anti* bridge modes). Adjacent chains are futher connected by 3,3′-Hbpt pillars to generate a 2D layer (Fig. 6e). From a topological perspective, both Ni1 and Ni2 act as the 4-connected node, tm can be viewed as 3-connected node and the 3,3′-bpt ligand can be viewed as the linker. In this way, this framework can be simplified to be a (3,4)-connected 2D layer architecture with the short Schläfli symbol of $(3.6^2)_2(3.4.6^2.7^2)_2(5.6^3.8^2)$ (Fig. 6f). Considering the trinuclear Ni(II) unit bridged by tm anions as a node to simply the structure of **6**, simplified topologie could also be determined with the short Schläfli symbol of $4^4.6^2$ (Fig. 6g). It is interesting that the lattice water molecules were embedded in the interlaced ABAB… arrangement model of 2D layer. The 3,3′-Hbpt ligands in **6** adopt two different bridging modes to link adjacent Ni atom (Fig. 6c). The intermolecular packing is further controlled by hydrogen bonds (Table S1) among the triazole N atoms, carboxylate O atoms and

water molecules, to generate a 3D supramolecular architecture.

Fig. 6

Structural Diversity of 1−6

It should be note that a variety of framework structures can be achieved on the basis of the choice of the aromatic tricarboxylate and triazole-containing dipyridyl isomers with differently oriented pyridyl groups as building blocks.[24] As a result, **1**−**5** form 3D network architecture and **6** form 2D layer architecture, with diversiform connectivity. The phenomenon of structural diversification in **1**−**6** may arise from some different sources in line with our previous work.[17] First of all, phenyl dicarboxylate ligands play an important role in constructing the polymer structures. These dicarboxylate isomers exhibit several coordination patterns (see Scheme 1), in which the carboxylate groups can adopt the bridging, unidentate and chelating modes, respectively. Secondly, the differently oriented pyridyl N atoms in these triazole-containing bpt isomers, which has a bent backbone, may play significant roles in the formation of different topological structures. Thirdly, metal-directing effect is also important for the structural diversity. In 2, the two Zn(II) centers adopt a slightly distorted trigonal-dipyramidal geometry and a tetrahedron geometry respectively. While in 4, two Cd(II) centers adopt slightly distorted octahedral geometry, the other two Cd(II) centers show distorted tetragonal-pyramidal geometry. The ionic radius of Cd(II) is longer than Zn(II), Co(II) and Cu(II) which means the Cd(II) center can adopt higher coordination numbers leading to a distinct polymeric framework. Different from reported, tm with three carboxylate groups exhibits more complicated coordination patterns. And the tm linker can be not only considered as bent building blocks like *o*-BDC, *m*-BDC, but also linear building blocks like *p*-BDC (Scheme 1). Furthermore, the triazolyl nitrogen atoms of the isomeric bpt ligands can provide potential coordination sites (in **3** and **4**), which is different from other bpt ligands act as links, may influence the final coordination architectures more complicated.[25]

Fluorescent Properties

In this paper, the luminescence spectra of compounds **1**-**4** in the solid state were studied at room temperature, and their emission spectra are depicted in Figure 7a. The

emission spectra have broad peaks with maxima at 426 nm (λ_{ex} = 371 nm), 464 nm (λ_{ex} = 411 nm), 367 nm (λ_{ex} = 310 nm) and 427 nm (λ_{ex} = 349 nm) for **1-4**, respectively, whereas the emission peaks for the free ligands 4,4′-Hbpt, 3,4′-Hbpt, and 3,3′-Hbpt were observed at 447 nm, 451 nm, and 488 nm (λ_{ex} = 368 nm, 378 nm, and 419 nm, respectively).[18d] The blue shifts of the luminescence emission maxima in **1-4** are presumably owing to the result of the coordination of the relevant ligands to a metal center, which effectively increases the rigidity and asymmetry of the ligands. [26]

Thermal Stabilities of the Compounds

Thermogravimetric analyses (TG) were carried out for complexes **1**−**6** and the results are shown in Figure 7b. The TGA curves of **1** suggest that the first weight loss of 16.47% in the region 65−302 °C corresponds to the release of the lattice water and coordinated water (calculated 16.94%), and then, a series of complicated weight losses were observed as the temperature increased until heating ends. For **2,** the complex is stable up to 379 °C, followed by a series of consecutive steps of weight loss that do not stop until heating ends. For **3**, the weight loss of the lattice water and the coordinated water (7.45%) occurs in the range of 80−213 °C (calculated 7.62%). The main framework remains intact until it is heated to 375 °C and then there are a series of complicated steps of weight loss that do not end until heating ends. For **4,** the first observed weight loss of 7.04 % in the region of 62–162 ^{o}C corresponds to the dehydration process (calculated 6.61 %). The residual framework starts to decompose owing to the expulsion of the lattice water and the coordinated water molecules beyond 162 ^{o}C with a series of complicated weight losses and does not stop until heating ends at 986 ^{o}C. For **5,** the first weight loss of 12.49% in the region of 65–210 ^{o}C corresponds to the release of the lattice water and the coordinated water molecules (calculated 12.19%). The residual framework starts to decompose beyond 210 ^{o}C with a series of complicated weight losses and does not stop until heating ends. For **6,** the weight loss of the lattice water and the coordinated water (10.59%) occurs in the range of 60−293 °C (calculated 10.82%). And then there are a series of complicated steps of weight loss that do not end until heating ends.

Fig. 7

Magnetic Properties

Magnetic susceptibility measurements were carried out on polycrystalline samples of **5** and **6** in the temperature range 2.0−300.0 K at 1000 Oe. For **5** (Fig 8a), the data above 30 K follow the Curie–Weiss law with C = 10.49 cm^3Kmol^{-1} and θ = -17.64 K. The $\chi_M T$ value at 300 K is 9.91 emu·K·mol^{-1}, which is much larger than the spin-only value 5.64 emu·K·mol^{-1} for three magnetically active Co(II) ions (S = 3/2, g = 2.0), as expected for Co(II) systems with a significant contribution from the effects of spin-orbital coupling. As the temperature is lowered, the $\chi_M T$ values decrease continuously and and reaches a local minimum of 5.96 emu·K·mol^{-1} at about 2 K, indicative of a strong single-ion behavior admixture with a weak antiferromagnetic interaction. [27]

Fig. 8

For **6**, (Fig 8b), the data above 2 K follow the Curie–Weiss law with C = 3.49 cm^3Kmol^{-1} and θ = 0.17 K. The $\chi_M T$ value at 300 K is 3.49 emu·K·mol^{-1}, which is in good agreement with the spin-only value 3.00 emu·K·mol^{-1} for three magnetically active Ni(II) ions (S = 1, g = 2.0). After lowering the temperature, the $\chi_M T$ value slightly increases to 3.53 emu·K·mol^{-1} at 30 K, then increases rapidly to reach a maximum of. 3.68 emu·K·mol^{-1} at 7 K, indicating a weak ferromagnetic coupling between the adjacent Ni(II) ions beidged by the *syn−anti* carboxylate groups. The final decrease of $\chi_M T$ may be attributed to the saturation effect, zero-field splitting of Ni(II) ions and/or the presence of anti-ferromagnetic interactions *via* exchange bridges between the adjacent Ni_3 units. No divergence between the zero-field-cooled (ZFC) and field-cooled (FC) magnetization, and thus no long-range magnetic ordering of **6** at low temperature (Fig S8 in the Supporting Information), was observed.

Conclusions.

In this paper, we have presented the synthesis and crystal structures of six coordination polymers generated from mixed-ligand systems of H_3tm and positional isomeric dipyridyl bridging ligands (4,4′-Hbpt, 3,4′-Hbpt and 3,3′-Hbpt), reacted with Zn(II), Cd(II), Co(II) and Ni(II) salts. The structural diversities indicate that the trimellitic acid (H_3tm) and the differently oriented pyridyl N atoms in these

triazole-containing bpt isomers, as well as the metal-directing effect play dominating roles in modulating the formation of structures of these crystalline materials. Different from our previous work[17], tm with three carboxylate groups exhibits more coordination patterns. And the tm linker can be act as bent building blocks like *o*-BDC, *m*-BDC and linear building blocks like *p*-BDC simultaneously. As a result, more diverse and interesting architectures than before were obtained: **1** and **5** both have a 3D 4-connected topology, with $(4.6^4.8)(4^2.6^3.8)_2(4^4.6^2)_2$ Schläfli symbol for **1** and $(4^2.5^2.7^2)(5^2.6^2.7.8)_2(4.5^2.6.7^2)_2$ symbol for **5**, respectively. **2** and **3** both have a 3D (4, 5)-topology, with $(3^4.4^2.5^2)_2(4^2.8^4)(3.4^3.5^2.6.7^2.8)_2$ Schläfli symbol for **2** and $(3^4.4^2.5^2)_2(4^2.8^4)(3.4^3.5^2.6.7^2.8)_2$ symbol for **3**, respectively. **4** has a 3D trinodal (3,4,5)-connected net with the short Schläfli symbol of $(3.4^4.5^3.6.7)(4^3.6^2.7)(4^4.6^2)(4^2.6)_2(4^5.6^4.8)_2$. **6** reveal a 2D (3,4)-connected layer with the short Schläfli symbol of $(3.6^2)_2(3.4.6^2.7^2)_2(5.6^3.8^2)$. Accordingly, our present findings will further enrich the crystal engineering strategy and offer the possibility of controlling the formation of the desired network structures.

Acknowledgment.

We gratefully acknowledge the National Nature Science Foundation of China (Nos. 21171101, 21101035, 21061002 and 90922032), Guangxi Natural Science Foundation of China (2012GXNSFBA053017, 2012GXNSFAA053035) and the Foundation of Key Laboratory for Chemistry and Molecular Engineering of Medicinal Resources.

References

1 (a) Y. K. Park, S. B. Choi, H. Kim, K. Kim, B. H. Won, K. Choi, J. S. Choi, W. S. Ahn, S. Kim, D. H. Jung, S. H. Choi, G. H. Kim, S. S. Cha, Y. H. Jhon, J. K. Yang, J. Kim, *Angew. Chem., Int. Ed*., 2007, **46**, 8230; (b) X.-Z. Wang, D.-R. Zhu, Y. Xu, J. Yang, X. Shen, J. Zhou, N. Fei, X.-K. Ke, L.-M. Peng, *Cryst. Growth Des*., 2010, **10**, 887; (c) A. Aijaz, E. C. Sa udo, P. K. Bharadwaj, *Cryst. Growth Des.*, 2011, **11**, 1122.

2 (a) I. G. Georgiev, L. R. MacGillivray, *Chem. Soc. Rev.*, 2007, **36**, 1239; (b) J. Yuasa, S. Fukuzumi, *J. Am. Chem. Soc*., 2008, **130**, 566; (c) F. M. Zhang, P. F. Yan, X. Y. Zou, J. W. Zhang, G. F. Hou, G. M. Li, *Cryst. Growth Des.*, 2014, **14**, 2014.

3 (a) Y.-Z. Zheng, W. Xue, M.-L. Tong, X.-M. Chen, F. Grandjean, G. J. Long, *Inorg. Chem.*, 2008, **47**, 4077; (b) H. Miyasaka, M. Julve, M. Yamashita, R. Clerac, *Inorg.*

Chem., 2009, **48**, 3420; (c) B. V. Harbuzaru, A. Corma, F. Rey, J. L. Jord, D. Ananias, L. D. Carlos, J. Rocha, *Angew. Chem., Int. Ed*., 2009, **48**, 6476.

4 (a) M. Kurmoo, *Chem. Soc. Rev*., 2009, **38**, 1353; (b) L. Armelaoa, S. Quici, F. Barigelletti, G. Accorsi, G. Bottarod, M. Cavazzini, E. Tondello, *Coord. Chem. Rev*., 2010, **254**, 487; (c) A. M. Kirillov, *Coord. Chem. Rev*., 2011, **255**, 1603; (d) B. Xu, J. Xie, H.-M. Hu, X.-L. Yang, F.-X. Dong, M.-L. Yang, G.-L. Xue, *Cryst. Growth Des.*, 2014, **14**, 1629.

5 (a) W.-J. Chuang, I.-J. Lin, H.-Y. Chen, Y.-L. Chang, C. N. H. Sodio, *Inorg. Chem.,* 2010, **49**, 5377; (b) P. Antunes, R. Delgado, M. G. B. Drew, V. Félix, Maecke, H. *Inorg. Chem.*, 2007, **46**, 3144; (c) P. J. Barnard, J. P. Holland, S. R. Bayly, T. J. Wadas, C. J. Anderson, J. R. Dilworth, *Inorg. Chem.*, 2009, **48**, 7117; (d) D. Jarzab, M. Lu, H. T. Nicolai, P. W. M. Blom, M. A. Loi, *Soft Matter*., 2011, **7**, 1702.

6 (a) R.-Q. Zou, A. I. Abdel-Fattah, H.-W. Xu, A. K. Burrell, T. E. Larson, T. M. McCleskey, Q. Wei, M. T. Janicke, D. D. Hickmott, T. V. Timofeeva, Y.-S. Zhao, *Cryst. Growth Des.* 2010, **10**, 1301; (b) X. Du, Y.-L. Sun, B.-E. Tan, Q.-F. Teng, X.-J. Yao, C.-Y. Su, W. Wang, *Chem. Commun.*, 2010, **46**, 970; (c) Y.-F. Zeng, J.-P. Zhao, B.-W. Hu, X. Hu, F.-C. Liu, J. Ribas, A. J. Ribas, X.-H. Bu, *Chem.Eur. J*., 2007, **13**, 9924; (d) D. K. Gale, C. Jeffryes, T. Gutu, J. Jiao, C.-H. Chang, G. L. Rorrer, *J. Mater. Chem*., 2011, **21**, 10658.

7 (a) W. Wei, M. Y.Wu, Y. G. Huang, Q. Gao, Q. F. Zhang, F. L. Jiang and M. C. Hong, *CrystEngComm*, 2009, **11**, 576; (b) J. J. Vittal, *Coord. Chem. Rev.* 2007, **251**, 1781. (d) Férey, G. Chem. Soc. Rev. 2008, **37**, 191; (c) J. P. Zhang, X. C. Huang, X. M. Chen, *Chem. Soc. Rev.* 2009, **38**, 2385; (d) J.-M. Lin, W.-B. Chen, X.-M. Lin, A.-H. Lin, C.-Y. Ma, W. Dong, C.-E. Tian, *Chem. Commun*., 2011, **47**, 2402.

8 (a) A. Y. Robin, K. M. Fromm, *Coord. Chem. Rev*., 2006, **250**, 2127; (b) Frontiers in Crystal Engineering; E. Tiekink, J. J. Vittal, Eds, John-Wiley & Sons Ltd.: New York, 2006; (c) N. L. Rosi, J. Kim, M. Eddaoudi, B. Chen, M. ÓKeeffe, O. M. Yaghi, *J. Am. Chem. Soc,*. 2005, **127**, 1504; (d) V.A. Blatov, M. ÓKeeffe, D. M. Proserpio, *CrystEngComm,* 2010, **12**, 44.

9 (a) S.-S. Zhang, S.-Z. Zhan, M. Li, R. Peng, D. Li, *Inorg. Chem.* 2007, **46**, 4365; (b) H.-X.Yang, J.-X. Lin, J.-T. Chen, X.-D. Zhu, S.-Y. Gao, R. Cao, *Cryst. Growth Des.* 2008, **8**, 2623; (c) Q.-R. Fang, G.-S. Zhu, Z. Jin, Y.-Y. Ji, J.-W. Ye, M. Xue, H. Yang, Y. Wang, S.-L. Qiu, *Angew. Chem., Int. Ed.* 2007, **46**, 6638; (d) X.-L Li,. K.

Chen, Y. Liu, Z.-X. Wang, T.-W. Wang, J.-L. Zuo, Y.-Z. Li, Y. Wang, J.-S. Zhu, J.-M. Liu, Y. Song, X.-Z. You, *Angew. Chem., Int. Ed.* 2007, **46**, 6820; (e) T. R. Cook, Y.-R. Zheng, and P. J. Stang, *Chem. Rev*. 2013, **113**, 734.

10 (a) R.-Q. Zou, H. Sakurai, S. Han, R.-Q. Zhong, Q. Xu, *J. Am. Chem. Soc.* 2007, **129**, 8402; (b) X. Y. Wang, Z. M. Wang, S. Gao, *Chem. Commun.* 2008, 281; (c) A.-J. Lan, K.-H. Li, H.-H. Wu, L.-Z. Kong, N. Nijem, D. H. Olson, T. J. Emge, Y. J. Chabal, D. C. Langreth, M.-C. Hong, J. Li, *Inorg. Chem.* 2009, **48**, 7165; (d) J. Zhang, S.-M. Chen, R. A. Nieto, T. Wu, P.-Y. Feng, X.-H. Bu, *Angew. Chem., Int. Ed.* 2010, **49**, 1267; (e) H.-Q. Hao, W.-T. Liu, W. Tan, Z.-J. Lin, M.-L. Tong, *Cryst. Growth Des.* 2009, **9**, 457.

11 (a) G. Zhang, G. Yang, Q. Chen, J.-S. Ma, *Cryst. Growth Des*., 2005, **5**, 661; (b) D.-F. Sun, R. Cao, Y.-Q. Sun, W.-H. Bi, D.-Q. Yuan, Q. Shi, X. Li, *Chem. Commun*., 2003, 1528.

12 (a) R. Heck, J. Bacsa, J.E. Warren, M.J. Rosseinsky, D. Bradshaw, *CrystEngComm* 2008, **10**, 1687; (b) L.-L. Qu, Y.-L. Zhu, Y.-Z. Li, H.-B. Du, X.-Z. You, *Cryst. Growth Des.* 2011, **11**, 2444; (c) C.-H. Li, K.-L. Huang, Y.-N. Chi, X. Liu, Z.-G. Han, L. Shen, C.-W. Hu, *Inorg. Chem.* 2009, **48**, 2010; (d) Y. Tao, J.-R. Li, Q. Yu, W.-C. Song, X.-L. Tong, X.-H. Bu, *CrystEngComm* 2008, **10**, 699.

13 (a) Y. Wang, X.-Q. Zhao, W. Shi, P. Cheng, D.-Z. Liao, S.-P. Yan, *Cryst. Growth Des*. 2009, **9**, 2137; (b) Y.-B. Lu, M.-S. Wang, W.-W. Zhou, G. Xu, G.-C. Guo, J.-S. Huang, *Inorg. Chem.* 2008, **47**, 8935; (c) B. Zheng, H. Dong, J. Bai, Y. Li, S. Li, M. Scheer, *J. Am. Chem. Soc.* 2008, **130**, 7778.

14 (a) M. J. Zaworotko, *Nature* 2008, **451**, 410; (b) M. Dinca, J. R. Long, *Angew. Chem. Int. Ed.* 2008, **47**, 6766; (c) S. Kitagawa, R. Matsuda, *Coord. Chem. Rev.* 2007, **251**, 2490; (d) S. Henke, R.A. Fischer, *J. Am. Chem. Soc.* 2011, **133**, 2064.

15 (a) H. Arora, F. Lloret, R. Mukherjee, *Inorg. Chem.* 2009, **48**, 1158; (b) H. Chun, H. Jung, J. Seo, *Inorg. Chem.* 2009, **48**, 2043; (c) Z. Chang, A.-S. Zhang, T.–L. Hu, X.–H. Bu, *Cryst. Growth Des.* 2009, **9**, 4840; (d) H. Kumagai, M. A. Tanaka, K. Inoue, K. Takahashi, H. Kobayashi, S. Vilminot, M. Kurmoo, *Inorg. Chem.* 2007, **46**, 5949.

16 (a) R. Robson, Comprehensive Supramolecular Chemistry, Pergamon, New York, 1996; (b) P. J. Hagrman, D. Hagrman and J. Zubieta, Angew. Chem., Int. Ed., 1999, **38**, 2639; (c) A. J. Blake, N. R. Champness, P. Hubberstey, W. S. Li, M. A.

Withersby and M. Schr€oder, Coord. Chem. Rev., 1999, **183**, 117; (d) S. Noro, R. Kitaura, M. Kondo, S. Kitagawa, T. Ishii, H. Matsuzaka and M. Yamashita, J. Am. Chem. Soc., 2002, **124**, 2568.

17 (a) F.-P. Huang, J.-L. Tian, W. Gu, X. Liu, S.-P. Yan, D.-Z. Liao, P. Cheng, *Cryst. Growth Des.* 2010, **10**, 1145; (b) F.-P. Huang, J.-L. Tian, G.-J. Chen, D.-D. Li, W. Gu, X. Liu, S.-P. Yan, D.-Z. Liao, P. Cheng, *CrystEngComm*. 2010, **12**, 1269; (c) F.-P. Huang, Z.-M. Yang, P.-F. Yao, Q. Yu, J.-L. Tian, H.-D. Bian, S.-P. Yan, D.-Z. Liao, P. Cheng, *CrystEngComm*. 2013, **15**, 2657.

18 Vyatsheslav, N. N.; Nikolay, V. Z.; Sergey, Z. V. ARKIVOC 2005,118.

19 SAINT Software Reference Manual; Bruker AXS: Madison, WI, 1998.

20 Sheldrick, G. M. Phase Annealing in SHELX-90: Direct Methods for Larger Structures. Acta Crystallogr. 1990, **A46**, 467.

21 Sheldrick, G. M. SHELXS-97, Program for X-ray Crystal Structure Solution; University of Göttingen: Göttingen, Germany, 1997.

22 (a) M. O'Keeffe and O. M. Yaghi, Reticular Chemistry Structure Resource; Arizona State University, Tempe, AZ, 2005 http:// okeeffews1.la.asu.edu/rcsr/ home.htm; (b) V. A. Blatov, Multipurpose crystallochemical analysis with the program package TOPOS, IUCr CompComm Newsletter, 2006, **7**, 4; (c) V. A. Blatov, A. P. Shevchenko and V. N. Serezhkin, *J. Appl. Crystallogr.*, 2000, **33**, 1193; (d) A. F. Wells, Three-Dimensional Nets and Polyhedra, Wiley Interscience, New York, 1977.

23 (a) Y. Yan, C.-D. Wu, X. He, Y.-Q. Sun, C.-Z. Lu, *Cryst. Growth Des.*, 2005, **5**, 821; (b) C. Qin, X.-L. Wang, L. Carlucci; M.-L. Tong; E.-B Wang; C.-W Hu*a* and X. Lin. *Chem. Commun.* 2004, 1876.

24 (a) M. Du, C.-P. Li , C.-S. Liu, S.-M. Fang, *Coord. Chem. Rev.,* 2013, **257**, 1282; (b) M. Du, X.-J. Jiang, X.-J. Zhao, *Inorg. Chem.*, 2007, **46**, 3984; (c) M. Du, X.-J. Jiang, X.-J. Zhao, *Inorg. Chem.*, 2006, **45**, 3998; (d) M. Du, X.-J. Jiang, X.-J. Zhao, *Chem. Commun,*. 2005, 5521; (e) M. Du, Z.-H. Zhang, Y.-P. You, X.-J. Zhao, CrystEngComm 2008, **10**, 306; (f) C.-P. Li, J. C., Q. Yu, M. Du, *Cryst. Growth Des.*, 2010, **10**, 1623.

25 (a) F.-P. Huang, J.-L. Tian, D.-D. Li, G.-J. Chen, W. Gu, S.-P. Yan, X. Liu, D.-Z. Liao, P. Cheng, *Inorg. Chem.* 2010, **49**, 2525; (b) F.-P. Huang, J.-L. Tian, D.-D. Li, G.-J. Chen, W. Gu, S.-P. Yan, X. Liu, D.-Z. Liao, P. Cheng, *CrystEngComm* 2010,

12, 395; (c) F.-P. Huang, J.-L. Tian, W. Gu, S.-P. Yan, *Inorg. Chem. Commun.* 2010, **13**, 90; (d) F.-P. Huang, Q. Zhang, Q. Yu, H.-D. Bian, H. Liang, S.-P. Yan, D.-Z. Liao, P. Cheng, *Cryst. Growth Des.* 2012, **12**, 1890; (e) F.-P. Huang, H. -Y. Li, Q. Yu, H.-D. Bian, J.- L. Tian, S.-P. Yan, D.-Z. Liao, P. Cheng, *CrystEngComm* 2012, **14**, 4756.

26 (a) Y.-C. Qiu, Y.-H. Li, G. Peng, J.-B. Cai, L.-M.Jin, L. Ma, H. Deng, M. Zeller, S. R. Batten, *Cryst. Growth Des.* 2010, **10**, 1332; (b) M.-X. Li, H. Wang, S.-W. Liang, M. Shao, X. He, Z.-X. Wang, S.-R. Zhu, *Cryst. Growth Des.* 2009, **9**, 4626; (c) X.-L. Tong, D.- Z. Wang, T.-L. Hu, W.-C. Song, Y. Tao, X.-H. Bu, *Cryst. Growth Des.* 2009, **9**, 2280; (d) Y. Li,; G. Xu,; W.-Q. Zou, M.-S. Wang, F.-K. Zheng, M.-F. Wu, H.-Y. Zeng, G.-C. Guo, J.-S. Huang, *Inorg. Chem*. 2008, **47**, 7945.

27 (a) L.-H. Jia, R.-Y. Li, Z.-M. Duan, S.-D. Jiang, B.-W. Wang, Z.-M. Wang, S. Gao, *Inorg. Chem.* 2011, **50**, 144; (b) N. Marino, O. F. Ikotun, M. Julve, F. Lloret, J. Cano, R. P. Doyle, *Inorg. Chem.* 2011, **50**, 378; (c) T. D. Keene, I. Zimmermann, A. Neels, O. Sereda, J. Hauser, M. Bonin, M. B. Hursthouse, D. J. Price, S. Decurtins, *Dalton Trans.* 2010, **39**, 4937; (d) S.-Q. Zang, X.-M. Ren, Y. Su, Y. Song, W.-J. Tong, Z.-P. Ni, H.-H. Zhao, S. Gao, Q.-J. Meng, *Inorg. Chem.* 2009, **48**, 9623; (e) L.-Q. Wei, B.-W. Li, S. Hu, M.-H. Zeng, *CrystEngComm,* 2011, **13**, 510.

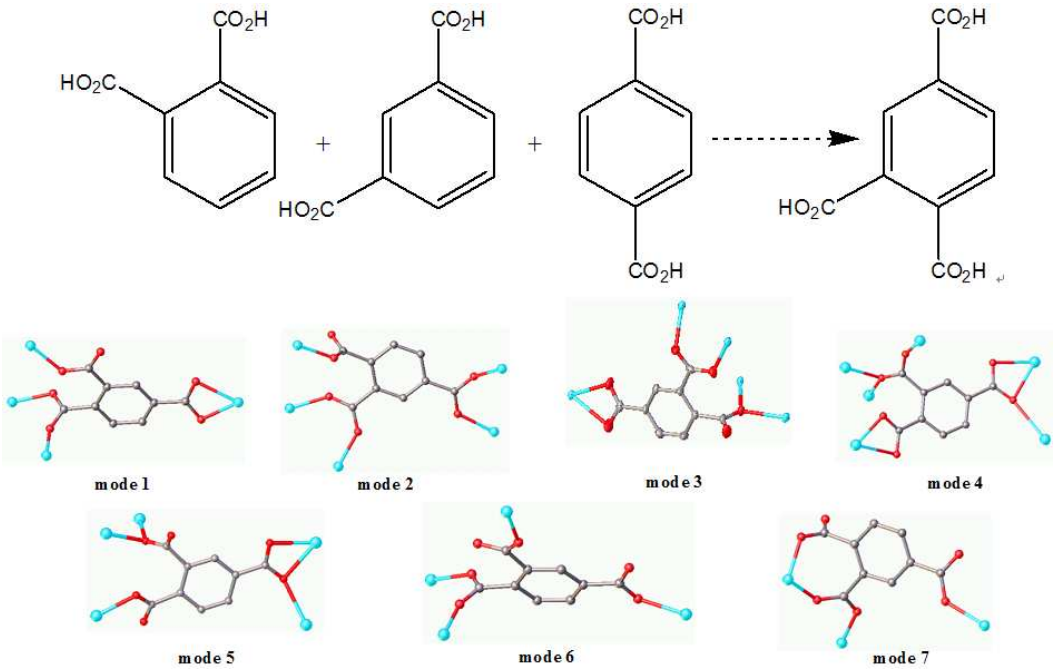

Scheme 1. The versatile coordination modes of tm used in this work.

Table 1 Crystal data and structure refinement for **1**–**6**.

Complex	**1**	**2**	**3**	**4**	**5**	**6**
Empirical formula	$C_{42}H_{48}N_{10}Zn_3O_{24}$	$C_{42}H_{24}N_{10}Zn_3O_{12}$	$C_{21}H_{17}Cd_2N_5O_9$	$C_{42}H_{28}Cd_4N_{10}O_{15}$	$C_{42}H_{40}Co_3N_{10}O_{20}$	$C_{66}H_{60}N_{20}Ni_3O_{21}$
Formula weight	1273.09	1056.88	708.22	1362.39	1181.63	1645.39
Crystal system	Monoclinic	Monoclinic	Triclinic	Triclinic	Triclinic	Triclinic
Space group	*C*2/*c*	*C*2/*c*	P-1	P-1	*P*-1	*P*-1
a (Å)	10.586 (2)	15.633 (3)	10.118 (2)	10.246 (2)	9.998 (2)	11.324 (2)
b (Å)	28.043 (8)	12.490 (3)	10.261 (2)	14.057 (3)	10.036 (2)	12.462 (3)
c (Å)	17.448 (3)	20.931 (4)	12.483 (3)	15.526 (3)	12.674 (3)	13.474 (3)
α (°)	90	90	113.43 (3)	109.87 (3)	96.16 (3)	78.55 (3)
β (°)	92.08 (3)	95.38 (3)	97.44 (3)	97.37 (3)	112.99 (3)	71.71 (3)
γ (°)	90	90	94.64 (3)	93.56 (3)	94.10 (3)	71.54
Volume ($Å^3$)	5176 (2)	4068.9 (2)	1166.6 (4)	2072.3 (7)	1155.0 (4)	1702.1 (6)
Z	4	4	2	2	1	1
Calculated density(Mg/m^3)	1.623	1.725	2.016	2.184	1.699	1.623
Goodness-of-fit on F^2	1.03	1.04	1.150	1.022	0.98	1.03
Independent reflections	4693	3670	4699	7428	4149	5872
$R_1[I>2\sigma(I)]$	0.057	0.061	0.055	0.070	0.052	0.109
wR_2 (all data)	0.145	0.116	0.143	0.1500	0.145	0.247

Table 2 Selected bond lengths (Å) and angles (º) for **1**–**6**.

1 (Symmetry codes: A: -*x*, *y*, -*z*+1/2; B: *x*-1, -*y*+1, *z*+1/2; C: -*x*+1/2, -*y*+1/2, -*z*+1.)

Zn1—O1	1.979 (3)	Zn1—N1	2.061 (4)	Zn2—N5B	2.097 (4)
Zn2—O5C	2.113 (4)	Zn2—O7	2.162 (4)	Zn2—O3A	1.997 (3)
Zn2—O2	2.144 (3)	Zn2—O6C	2.258 (3)		
O1A—Zn1—O1	134.0 (2)	O1—Zn1—N1A	103.2 (2)	O1—Zn1—N1	103.3 (2)
O1A—Zn1—N1A	103.3 (2)	O1A—Zn1—N1	103.2 (2)	N1A—Zn1—N1	108.2 (2)
O3A—Zn2—N5B	98.17 (2)	O7—Zn2—O6C	89.65 (2)	O5C—Zn2—O2	92.45 (2)
O3A—Zn2—O5C	106.53(2)	O5C—Zn2—O7	88.25 (2)	O3A—Zn2—O7	91.87 (2)
N5B—Zn2—O5C	155.30(2)	O2—Zn2—O7	177.4 (2)	N5B—Zn2—O7	91.13 (2)
O3A—Zn2—O2	85.50 (2)	O3A—Zn2—O6C	166.5 (2)	O5C—Zn2—O6C	60.14 (2)
N5B—Zn2—O2	89.30 (2)	N5B—Zn2—O6C	95.18 (2)	O2—Zn2—O6C	92.90 (2)

2 (Symmetry codes: A: *x*+1/2, *y*-1/2, *z*; B: -*x*+3/2, -*y*+3/2, -*z*+1; C: *x*-1/2, *y*+1/2, *z*; D: -*x*+3/2, *y*+1/2, -*z*+3/2; E: -*x*+1, *y*, -*z*+3/2.)

Zn1—O5A	1.999 (3)	Zn1—O1	2.025 (4)	Zn1—N1	2.140 (5)
Zn1—O6B	2.021 (4)	Zn1—N5B	2.137 (5)	Zn2—O3	1.947 (4)
Zn2—O2C	1.942 (4)	Zn2—O2D	1.942 (4)	Zn2—O3E	1.947 (4)
O5A—Zn1—O6B	133.45(2)	O5A—Zn1—N5B	88.93 (2)	O5A—Zn1—N1	90.98 (2)
O5A—Zn1—O1	135.29(2)	O6B—Zn1—N5B	88.13 (2)	O6B—Zn1—N1	92.42 (2)
O6B—Zn1—O1	91.11 (2)	O1—Zn1—N5B	89.25 (2)	O1—Zn1—N1	90.34 (2)
N5B—Zn1—N1	179.3 (2)	O2D—Zn2—O3E	112.1 (2)	O2D—Zn2—O3	112.4 (2)
O2C—Zn2—O2D	102.6 (3)	O2C—Zn2—O3	112.1 (2)	O3E—Zn2—O3	105.4 (2)
O2C—Zn2—O3E	112.4 (2)				

3 (Symmetry codes: (A) −*x*+1, −*y*+1, −*z*; (B) *x*, *y*+1, *z*; (C) −*x*+1, −*y*+1, −*z*+1; (D) −*x*, −*y*+2, −*z*.)

Cd1—N1A	2.366 (6)	Cd1—O4B	2.219 (5)	Cd2—O3B	2.283 (5)
Cd1—N3	2.398 (6)	Cd1—O5C	2.293 (5)	Cd2—O5C	2.310 (5)
Cd1—O1	2.270 (5)	Cd2—N4	2.320 (6)	Cd2—O7	2.322 (5)
Cd1—O2	2.511 (6)	Cd2—N5D	2.319 (6)	Cd2—O8	2.300 (6)
N1i—Cd1—N3	78.3 (2)	O4B—Cd1—O2	88.1 (2)	O3B—Cd2—O5C	88.7 (2)
N1i—Cd1—O2	86.2 (2)	O4B—Cd1—O5C	87.0 (2)	O3B—Cd2—O7	174.8 (2)
N3—Cd1—O2	139.5 (2)	O5C—Cd1—N1A	146.2 (2)	O3B—Cd2—O8	97.0 (2)
O1—Cd1—N1A	105.9 (2)	O5C—Cd1—N3	80.5 (2)	O5C—Cd2—N4	86.1 (2)
O1—Cd1—N3	94.4 (2)	O5C—Cd1—O2	126.3 (2)	O5C—Cd2—N5D	170.2 (2)
O1—Cd1—O2	54.2 (2)	N4—Cd2—O7	87.3 (2)	O5C—Cd2—O7	96.6 (2)
O1—Cd1—O5C	101.7 (2)	N5D—Cd2—N4	103.1 (2)	O8—Cd2—N4	168.0 (2)
O4B—Cd1—N1A	85.0 (2)	N5D—Cd2—O7	87.3 (2)	O8—Cd2—N5D	84.4 (2)
O4B—Cd1—N3	126.8 (2)	O3B—Cd2—N4	92.7 (2)	O8—Cd2—O5C	87.1 (2)
O4B—Cd1—O1	138.8 (2)	O3B—Cd2—N5D	87.6 (2)	O8—Cd2—O7	83.7 (2)

4 (Symmetry codes: A: *x*−1, *y*, *z*; B: −*x*+2, −*y*+1, −*z*+1; C: *x*+1, *y*, *z*; D: −*x*, −*y*, −*z*; E: −*x*+2, −*y*+2, −*z*+1.)

Cd1—O4A	2.234 (7)	Cd2—O8	2.287 (7)	Cd3—O7	2.506 (7)
Cd1—N1	2.261 (8)	Cd2—O13	2.303 (9)	Cd4—N8	2.186 (9)

Cd1—O1	2.292 (8)	Cd2—O4A	2.334 (7)	Cd4—O5A	2.202 (7)
Cd1—O3B	2.329 (7)	Cd2—O7	2.454 (7)	Cd4—N10E	2.233 (9)
Cd1—O2	2.410 (8)	Cd3—N4	2.192 (8)	Cd4—O15	2.402(13)
Cd1—O9C	2.412 (7)	Cd3—O11C	2.202 (7)	Cd4—O6A	2.535 (8)
Cd2—O9C	2.213 (7)	Cd3—N5D	2.288 (9)	Cd4—O2	2.777 (8)
Cd2—N6	2.260 (9)	Cd3—O14	2.338 (9)		
O4A—Cd1—N1	95.2 (3)	N6—Cd2—O13	91.6 (4)	O11C—Cd3—O7	88.3 (3)
O4A—Cd1—O1	161.2 (3)	O8—Cd2—O13	92.1 (3)	N5D—Cd3—O7	83.0 (3)
N1—Cd1—O1	94.8 (3)	O9C—Cd2—O4A	75.3 (3)	O14—Cd3—O7	160.8(3)
O4A—Cd1—O3B	103.7 (3)	N6—Cd2—O4A	105.9(3)	N8—Cd4—O5A	131.4(3)
N1—Cd1—O3B	93.2 (3)	O8—Cd2—O4A	94.6 (3)	N8—Cd4—N10E	108.3(3)
O1—Cd1—O3B	91.6 (3)	O13—Cd2—O4A	160.8(3)	O5A—Cd4—N10E	114.7(3)
O4A—Cd1—O2	110.4 (3)	O9C—Cd2—O7	107.9(3)	N8—Cd4—O15	97.0 (4)
N1—Cd1—O2	149.5 (3)	N6—Cd2—O7	148.2(3)	O5A—Cd4—O15	112.9(4)
O1—Cd1—O2	56.2 (3)	O8—Cd2—O7	55.7 (3)	N10E—Cd4—O15	77.9 (4)
O3B—Cd1—O2	96.4 (3)	O13—Cd2—O7	82.3 (3)	N8—Cd4—O6A	93.8 (3)
O4A—Cd1—O9C	73.4 (2)	O4A—Cd2—O7	86.7 (3)	O5A—Cd4—O6A	54.9 (3)
N1—Cd1—O9C	87.5 (3)	N4—Cd3—O11B	127.2(3)	N10E—Cd4—O6A	152.7(3)
O1—Cd1—O9C	91.2 (3)	N4—Cd3—N5D	115.5(3)	O15—Cd4—O6A	83.7 (4)
O3B—Cd1—O9C	177.0 (3)	O11C—Cd3—N5D	116.0(3)	N8—Cd4—O2	92.0 (3)
O2—Cd1—O9C	84.4 (3)	N4—Cd3—O14	97.5 (3)	O5A—Cd4—O2	77.2 (3)
O9C—Cd2—N6	103.5 (3)	O11C—Cd3—O14	103.3(3)	N10E—Cd4—O2	76.7 (3)
O9C—Cd2—O8	161.8 (3)	N5D—Cd3—O14	78.2 (3)	O15—Cd4—O2	154.6(3)
N6—Cd2—O8	93.6 (3)	N4—Cd3—O7	87.0 (3)	O6A—Cd4—O2	119.4(2)
O9C—Cd2—O13	93.2 (3)				

5 (Symmetry codes: A: -*x*+2, -*y*, -*z*+1; B: *x*-1, *y*, *z*; C: -*x*+3, -*y*, -*z*+1; D: -*x*+2, -*y*-1, -*z*+1; E: -*x*+1, -*y*, -*z*; F: *x*+1, *y*-1, *z*+1; G: -*x*+2, -*y*, -*z*.)

Co1—O1	2.048 (3)	Co1—O6B	2.078 (3)	Co1—O7	2.145 (3)
Co2—O2	2.071 (3)	Co2—O8	2.137 (3)	Co2—N5E	2.125 (4)
Co3—O3	2.069 (3)	Co3—N1	2.123 (4)	Co3—O9	2.147 (3)
O1—Co1—O7	94.47 (1)	O1—Co1—O6C	89.71 (1)	O1A—Co1—O7	85.53 (1)
O6B—Co1—O7	90.77 (1)	O6B—Co1—O7A	89.23 (1)	O7—Co1—O7A	180.00
O2—Co2—O8	83.24 (1)	N5E—Co2—O8	89.40 (1)	O2D—Co2—N5E	88.27 (1)
O2—Co2—N5E	91.73 (1)	O2D—Co2—O8	96.76 (1)	N5E—Co2—N5F	180.00
O3—Co3—N1	88.39 (4)	O3—Co3—O9	95.65 (3)	N1—Co3—O9	89.31 (4)
O3—Co3—N1G	91.61 (4)	O3—Co3—O9G	84.35 (3)	N1G—Co3—N1	180.00

6 (Symmetry codes: (A) −*x*+1, −*y*+2, −*z*; (B) −*x*, −*y*+2, −*z*+1; (C) *x*+1, *y*+1, *z*−1; (D) −*x*+1, −*y*+3, −*z*.)

Ni1—N1	2.130 (8)	Ni1—O4A	2.027 (6)	Ni2—O3	2.074 (6)
Ni1—N5A	2.131 (7)	Ni1—O7	2.111 (6)	Ni2—O3D	2.074 (6)
Ni1—N6	2.105 (7)	Ni2—N10B	2.089 (7)	Ni2—O5	2.088 (7)
Ni1—O1	2.096 (6)	Ni2—N10C	2.089 (7)	Ni2—O5D	2.088 (7)

N1—Ni1—N5A	173.3 (3)	O4A—Ni1—N6	96.4 (3)	O3—Ni2—O3D	180
N6—Ni1—N1	97.9 (3)	O4A—Ni1—O1	86.5 (2)	O3—Ni2—O5D	88.5 (3)
N6—Ni1—N5A	88.2 (3)	O4A—Ni1—O7	173.2 (2)	O3D—Ni2—O5	88.5 (3)
N6—Ni1—O7	89.6 (3)	O7—Ni1—N1	91.3 (3)	O3—Ni2—O5	91.5 (3)
O1—Ni1—N1	86.8 (3)	O7—Ni1—N5A	91.5 (3)	O3D—Ni2—O5D	91.5 (3)
O1—Ni1—N5A	87.2 (3)	N10B—Ni2—N10C	180	O5—Ni2—N10C	86.8 (3)
O1—Ni1—N6	174.4 (3)	O3—Ni2—N10C	87.8 (3)	O5D—Ni2—N10C	93.2 (3)
O1—Ni1—O7	87.3 (2)	O3D—Ni2—N10B	87.8 (3)	O5D—Ni2—N10B	86.8 (3)
O4A—Ni1—N1	91.1 (3)	O3D—Ni2—N10C	92.2 (3)	O5—Ni2—N10B	93.2 (3)
O4A—Ni1—N5A	85.4 (3)	O3—Ni2—N10B	92.2 (3)	O5—Ni2—O5D	180

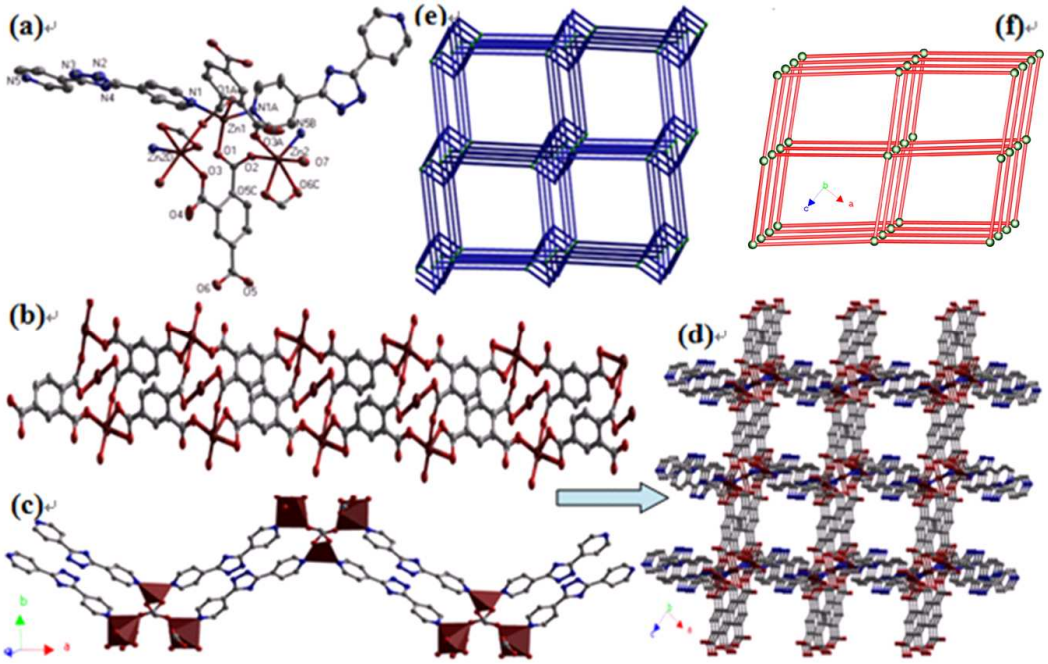

Fig. 1 Structural characterization of **1:** (a) the local coordination environments of the Zn(II) atoms (Symmetry codes: A: -*x*, *y*, -*z*+1/2; B: *x*-1, -*y*+1, *z*+1/2; C: -*x*+1/2, -*y*+1/2, -*z*+1.); (b) the 1D $[Zn(tm)]_{\infty}$ chain; (c) the 1D $[Zn(4,4'\text{-Hbpt})]_{\infty}$ chain; (d) the 3D pillared network; (e) the schematic description for the 3D architecture with $(4.6^4.8)(4^2.6^3.8)_2(4^4.6^2)_2$ symbol; (f) the simplified topologie with $5^2.6^4$ considering the trinuclear Zn(II) unit as a node.

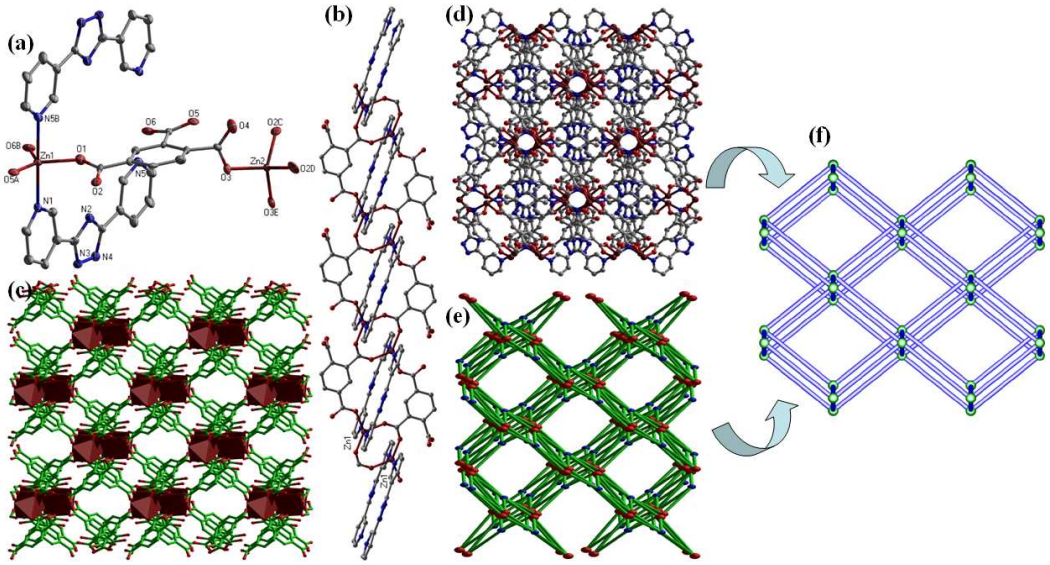

Fig. 2 Structural characterization of **2:** (a) the local coordination environments of the Zn(II) atoms (Symmetry codes: A: *x*+1/2, *y*-1/2, *z*; B: -*x*+3/2, -*y*+3/2, -*z*+1; C: *x*-1/2, *y*+1/2, *z*; D: -*x*+3/2, *y*+1/2, -*z*+3/2; E: -*x*+1, *y*, -*z*+3/2.); (b) the 1D chain along the *c* axis bridged by tm and 3,3′-Hbpt connector; (c) the 3D $[Zn(tm)]_{\infty}$ network; (d) the 3D pillared architecture of **2**; (e) the schematic description for the 3D architecture; (f) the simplified topologie with $(4^4.6^2)(4^8.6^6.8)$ considering the dinuclear Zn(II) unit as a node.

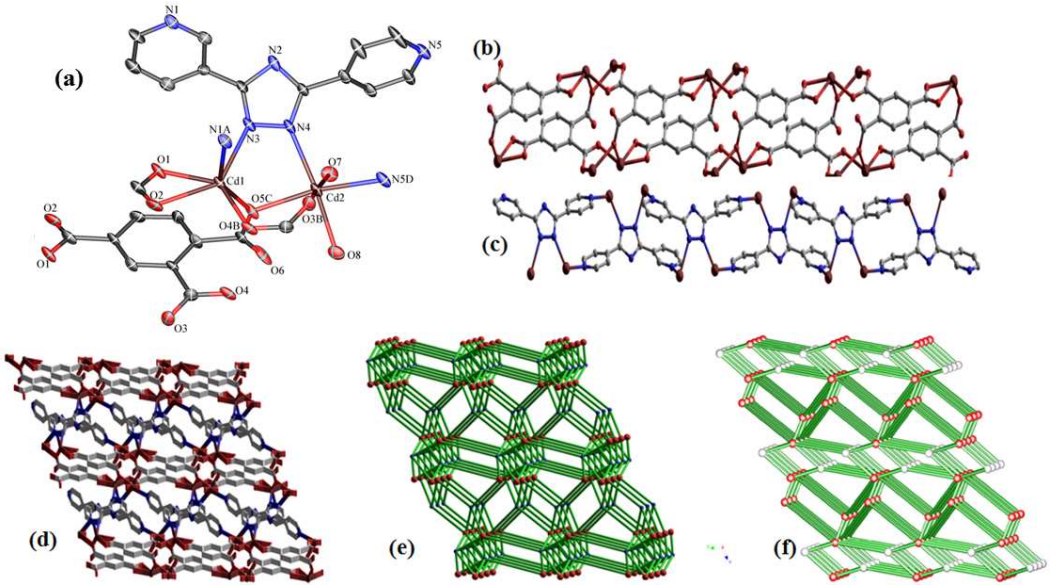

Fig. 3 Structure of **3** showing (a) the local coordination environments of the Cd(II) atoms (Symmetry codes: (A) −*x*+1, −*y*+1, −*z*; (B) *x*, *y*+1, *z*; (C) −*x*+1, −*y*+1, −*z*+1; (D) −*x*, −*y*+2, −*z*.), (b) the 1D chain bridged by tm, (c) the 1D chain bridged by the 3,4′-bpt, (d) View of the 3D novel (4,5)-connected

pillared architecture of **3**, (e) its schematic description; (f) the simplified topologie with $(4^2.6)(4^2.6^5.8^3)$ considering the dinuclear Cd(II) unit as a node.

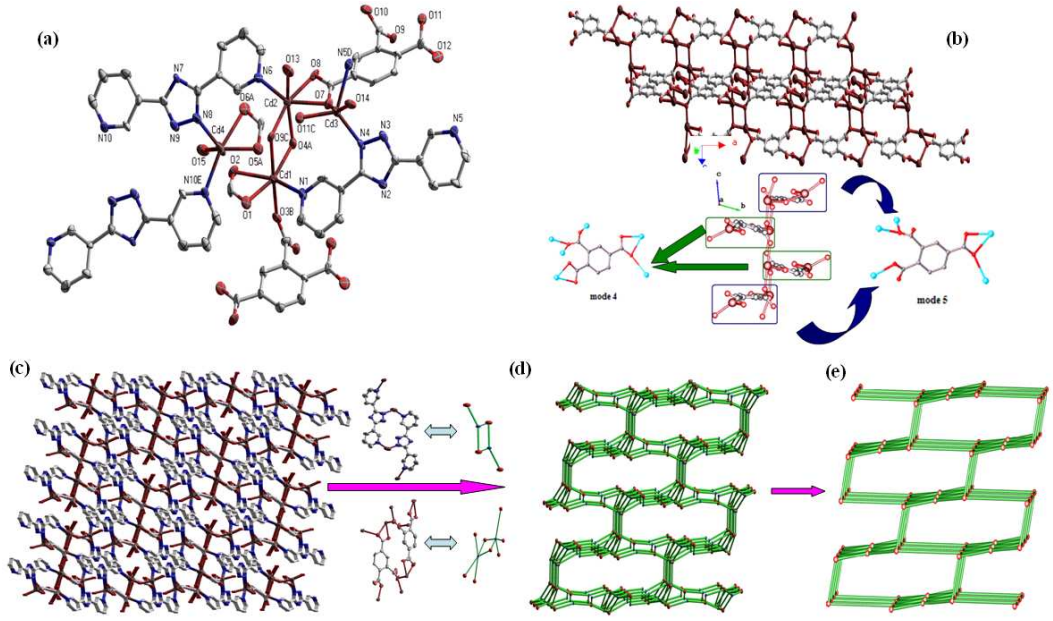

Fig. 4 (a) Structure of **4** showing the local coordination environments of the Cd(II) atoms (Symmetry codes: A: *x*−1, *y*, *z*; B: −*x*+2, −*y*+1, −*z*+1; C: *x*+1, *y*, *z*; D: −*x*, −*y*, −*z*; E: −*x*+2, −*y*+2, −*z*+1.); (b) the 1D chain formed by tm bridged Cd(II) coordination polymer; (c) View of the 3D (3,4,5)-connected architecture; (d) its schematic description of the "brick-wall"-like network; (e) the simplified topologie with $(3^2.4^2.5^2)$ $(3^2.4^5.5^6.6^2)_2$ considering the dinuclear Cd(II) unit as a node.

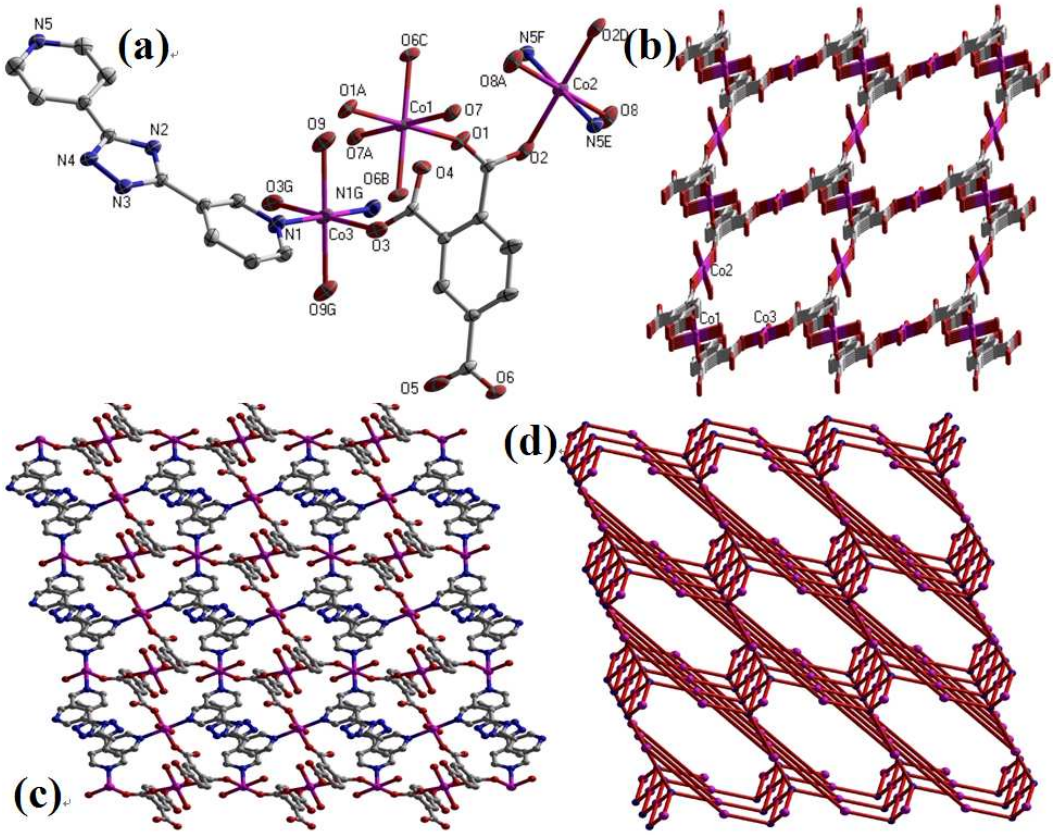

Fig. 5. View of (a) the local coordination environments of the Co(II) atoms(Symmetry codes: A: -*x*+2, -*y*, -*z*+1; B: *x*-1, *y*, *z*; C: -*x*+3, -*y*, -*z*+1; D: -*x*+2, -*y*-1, -*z*+1; E: -*x*+1, -*y*, -*z*; F: *x*+1, *y*-1, *z*+1; G: -*x*+2, -*y*, -*z*.); (b) the 2D $[Co(tm)]_{\infty}$ layer and (c) the 3D four-connected pillared architecture of **5** and (d) its schematic description.

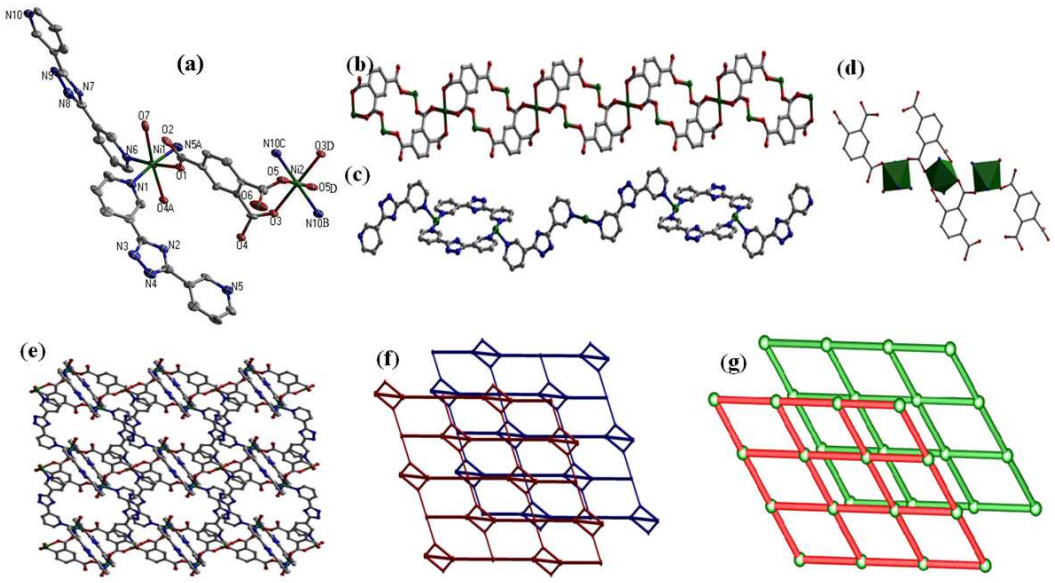

Fig. 6 View of (a) the local coordination environments of the Ni(II) atoms (Symmetry codes: Symmetry codes: (A) $-x+1, -y+2, -z$; (B) $-x, -y+2, -z+1$; (C) $x+1, y+1, z-1$; (D) $-x+1, -y+3, -z$.); (b) the 1D $[Ni(tm)]_{\infty}$ chain and (c) the 1D $[Ni(3,3'\text{-Hbpt})]_{\infty}$ chain; (d) the Ni_3 subunit; (e) the 2D architecture of **6** and (f) its schematic description; (f) the simplified topologie with $4^4.6^2$ considering the trinuclear Ni(II) unit unit as a node.

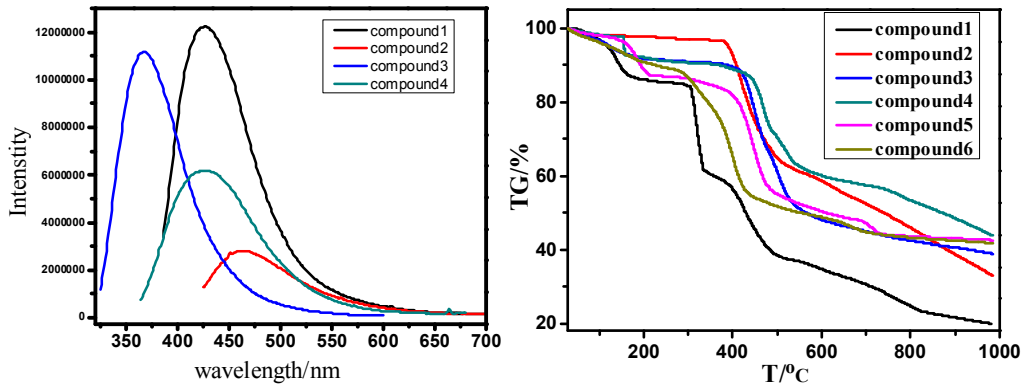

(a) (b)

Fig. 7. (a) The solid-state emission spectra of **1**–**4** at room temperature; (b) The TG curves of compounds **1**−**6**.

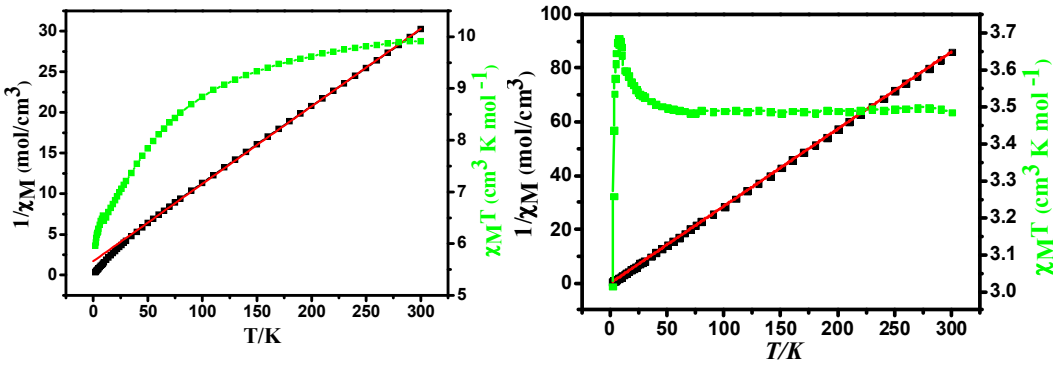

(a) (b)

Fig. 8 Plots of $\chi_M T$ *vs.* T (blue) and $1/\chi_M$ *vs.* T (black) for **5** (a) and **6** (b), the lines across $1/\chi_M$ curves represent the best fit.